Preprints (www.preprints.org) | NOT PEER-REVIEWED | Posted: 23 November 2017 doi:10.20944/preprints201711.0154.v1

Article

Modeling and Analysis of Opto-Fluidic Sensor for Lab-On- a-Chip Application

Venkatesha M. 1*, Chaya B. M. 1, Pattnaik P. K. 2 and Narayan K. 1

[1] Sai Vidya Institute of Technology, Bengaluru, Karnataka, India; venkatesha.m@saividya.ac.in
[2] BITS-Pilani, Hyderabad campus, Hyderabad, India.

* Correspondence: venkatesha.m@saividya.ac.in; Tel.: +91-897-113-7161

Abstract: In this work modeling and analysis of an integrated opto-fluidic sensor, with a focus on achievement of single mode optical confinement and continuous flow of micro particles in the microfluidic channel for Lab-on-a Chip (LOC) sensing application is presented. This sensor consists of integrated optical waveguides, microfluidic channel among other integrated optical components. A continuous flow of micro particles in a narrow fluidic channel is achieved by maintaining the two sealed chambers at different temperatures and by maintaining a constant pressure of 1Pa at the centroid of narrow fluidic channel geometry. The analysis of silicon on insulator (SOI) integrated optical waveguide at an infrared wavelength of 1550nm for single mode sensing operation is presented. The optical loss is found to be 0.0005719dB/cm with an effective index of 2.2963. The model presented in this work can be effectively used to detect the nature of micro particles and continuous monitoring of pathological parameters for sensing applications.

Keywords: micro fluidic channel; micro particles; fluid flow rate; lab-on-a-chip; waveguide

1. Introduction

A Lab-On-a-Chip (LOC) is a device that integrates many laboratory tests on a common integrated circuit. The size of LOC is in the range of few millimeters to few square centimeters [1]. LOC's requires the combination of microfluidics, manipulation and study of micro liters of fluids and light-fluid interaction. Most of the LOC fabrication processes were developed on silicon. Silicon fabrication processes are directly derived from semiconductor fabrication. The demands for cheap and easy production of LOC's results in a simple technology for the development of polydimethylsiloxane (PDMS), microfluidic devices [2]. LOC's provides application related advantages such as low fluid volume consumption, faster analysis, quick response times and compactness of the system due to the integration of multiple functions [3].

In most of the opto-fluidic sensors used in LOC applications, the sensitivity and accurate test results depends on microfluidics, light-fluid interaction and light guiding properties of optical waveguide. Microfluidics involves behavior, control and manipulation of fluids that are geometrically constrained to a millimeter scale. At small scales (channel size around 100nm to 500µm), the comparison between effects of the momentum of a fluid to that of viscosity is given by Reynolds number and its value can become very low. At lower Reynolds number, fluid flow becomes laminar and molecular transportation occurs due to diffusion [4]. Accurate specifications in chemical and physical properties such as temperature, concentration and pressure results in more uniform reaction conditions and more accurate single or multi step reactions [5,6]. In this article the optical waveguides and microfluidic channel are developed by using silicon as guiding medium. Silicon is transparent to infrared light with wavelengths above 1100nm [7]. In the development of biosensors, the bio-sample flow rate plays a very important role in its sensitivity. The sensitivity of ultrasensitive and selective non-enzyme using copper wires is found to be high at near infrared region [8]. Electrochemical detection of glucose from whole blood using copper wires [9], radio

Preprints (www.preprints.org) | NOT PEER-REVIEWED | Posted: 23 November 2017 doi:10.20944/preprints201711.0154.v1

frequency [10], and capillary based ring resonators [11] is presented with many other sensing mechanisms [12-17].

Figure 1 shows schematic of an integrated opto-fluidic biosensor employed for modeling and simulation. It consists of a laser source at 1550nm, photo detector and SOI input and output waveguides (shown in Red color) with a narrow fluidic channel (Shown in blue color). In the operation, the optical power is coupled into the input waveguide by using laser source (1550nm). The guided modes propagate through the input waveguide and couples into the fluidic sensing region. When the light couples from input waveguide to the output waveguide through the fluidic sample the absorption of optical power occurs due to the properties of the micro particles present in the fluidic sample. Based on the fluidic gap distance, a mode mismatch occurs between fluidic gap and input waveguide. Mode mismatch occurs due to the absorption of optical power [18], in fluidic gap. Hence mode mismatch which occurs during propagation of light through sensing region (fluidic gap distance) and absorption of optical power by the analyte is used for the purpose of analysis and also as a designing tool

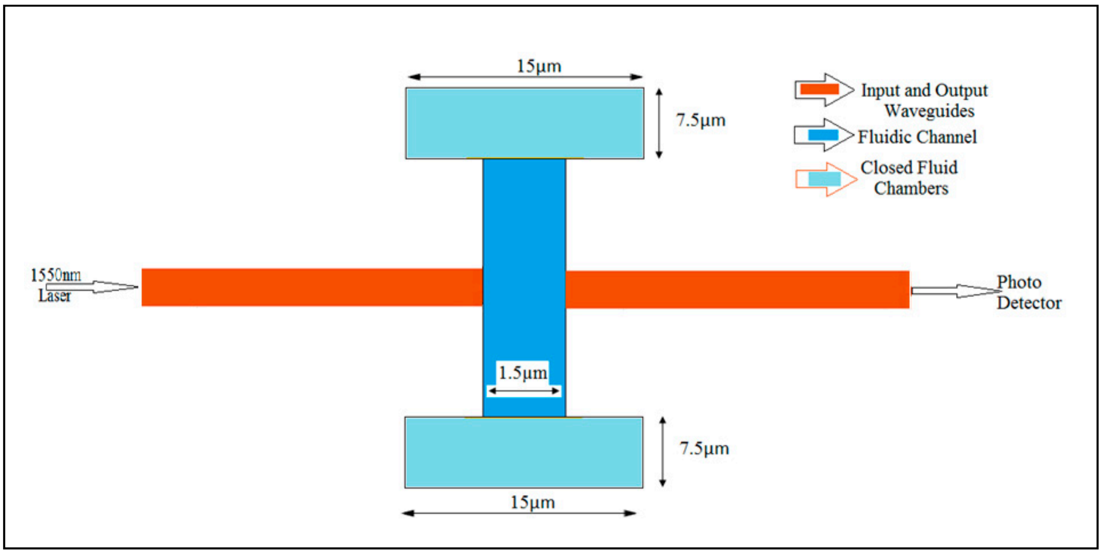

Figure 1: Schematic representation Integrated Biosensor

In this article modelling of micro fluidic channel to achieve a continuous flow rate between two sealed chambers maintained at different temperatures and pressure acting on the fluidic channel walls is described in section two. The modelling and modal analysis of SOI waveguides for use in light propagation is discussed in section three. The optical properties of SOI waveguide at infrared wavelength range 1500nm to 1600nm and power coupling analysis is depicted in section four.

2. Modeling of Micro Fluidic Channel

In this section microfluidic structure shown by blue color in Figure 1 is designed and analyzed. Micro fluidic channels are small dimension structures developed to achieve flow rate, sorting and manipulation of fluids that are geometrically constrained.

Figure 2 shows the structure of micro fluidic channel used for analyzing the flow rate between the two closed fluidic chambers, which are maintained at different temperatures. It consists of two fluidic chambers having dimensions of 7.5µm in length and 15µm in depth. The fluidic chambers are linked by a narrow channel having 1.5µm width and 15µm in length. The chamber and channel walls are modeled using silicon as material having a thickness of 1µm. The walls of the two chambers are in thermal contact with heat sinks maintained at 290 K and 300 K, respectively. The

Preprints (www.preprints.org) | NOT PEER-REVIEWED | Posted: 23 November 2017 doi:10.20944/preprints201711.0154.v1

channel walls are thermally insulated. The fluid in the center of the channel is maintained at a pressure of 1 Pascal.

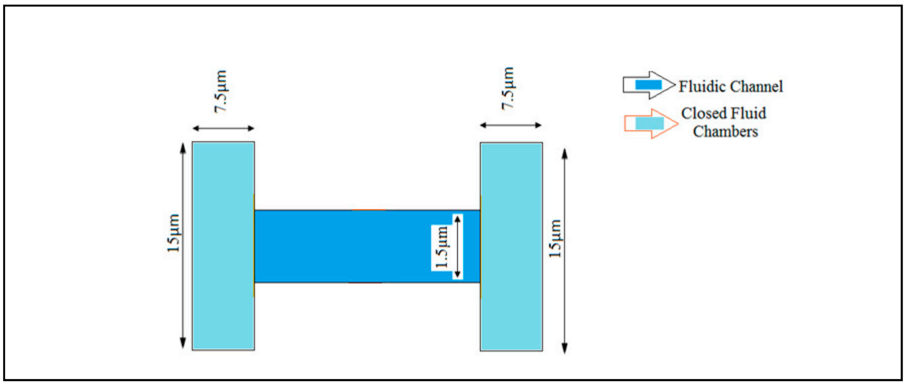

Figure 2: Structure of micro fluidic channel

The micro fluidic channel shown in figure 2 is used to compute the flow between two sealed chambers (closed fluid chambers) connected by a micro-channel with conducting walls when the chambers are maintained at different temperatures. The material used for the walls is Silicon. To achieve a continuous flow rate between two sealed chambers a birefringent object is used with a pressure point at the centroid of channel geometry. For channels of micron scale dimensions the Knudsen number becomes larger than 0.01. At atmospheric pressure, it is therefore necessary to use a slip condition on the surfaces of walls in the vicinity of the channel. The slip velocity, u_{slip}, along the walls of the micro fluidic channel is given by equations (1) and (2) [19].

$$u_{slip} = \sigma_s \frac{\lambda}{\mu}\left(\tau n - \left(\left(n^T \tau n\right)n\right)\right) + \sigma_T \frac{\mu}{\rho T_F}\left[\nabla T_W - \left(n.\nabla T_W\right)n\right] \quad (1)$$

$$T_W = T_F - \zeta_T \lambda_n.\nabla.T \quad (2)$$

Where, λ is the mean free path of the fluid, n is the boundary normal, τ is the viscous stress tensor, T_W is the wall temperature, T_F is the temperature of the fluid, μ is its viscosity, and ρ is its density. The slip coefficients, σ_s is the viscous slip coefficient, σ_T is the thermal slip coefficient, and ζ_T is the temperature jump coefficient can be defined by material properties, a_v is the tangential momentum accommodation coefficient. The slip coefficients are given by equation (3), (4) and (5) [20].

$$\sigma_S = \frac{2 - a_v}{a_v} \quad (3)$$

$$\sigma_T = \frac{3}{4} \quad (4)$$

$$\zeta_T = 2\frac{2 - a_v}{a_v}\frac{\gamma}{\gamma + 1}\frac{\kappa}{\mu C_P} \quad (5)$$

Where κ the thermal conductivity of fluid and the mean free path can be computed from the fluid properties using the following equation (6) and (7) [21].

Preprints (www.preprints.org) | NOT PEER-REVIEWED | Posted: 23 November 2017 doi:10.20944/preprints201711.0154.v1

$$\lambda = \frac{1}{C_O}\frac{\mu}{\rho\langle c\rangle} \tag{6}$$

$$\langle c\rangle = \sqrt{\left(\frac{8RT}{\pi M_n}\right)} = \sqrt{\frac{8p}{\pi\rho}} \tag{7}$$

A continuous flow between the two sealed chambers maintained at slightly different temperatures is achieved by maintaining a pressure of 1 pa at the centroid of micro fluidic geometry. The channel width is 1.5μm, so the Knudsen number varies from 0.064 and 0.045.

The relative pressure acting on the channel wall, as a function of position along the wall is represented by mean path of micro particles. As the absolute pressure in a fluid flow is reduced, the mean free path of the fluid molecules begins to approach the size of the vessel through, which, the flow occurs. The detailed analysis of the velocity magnitude, Pressure and temperature analysis is described in this section.

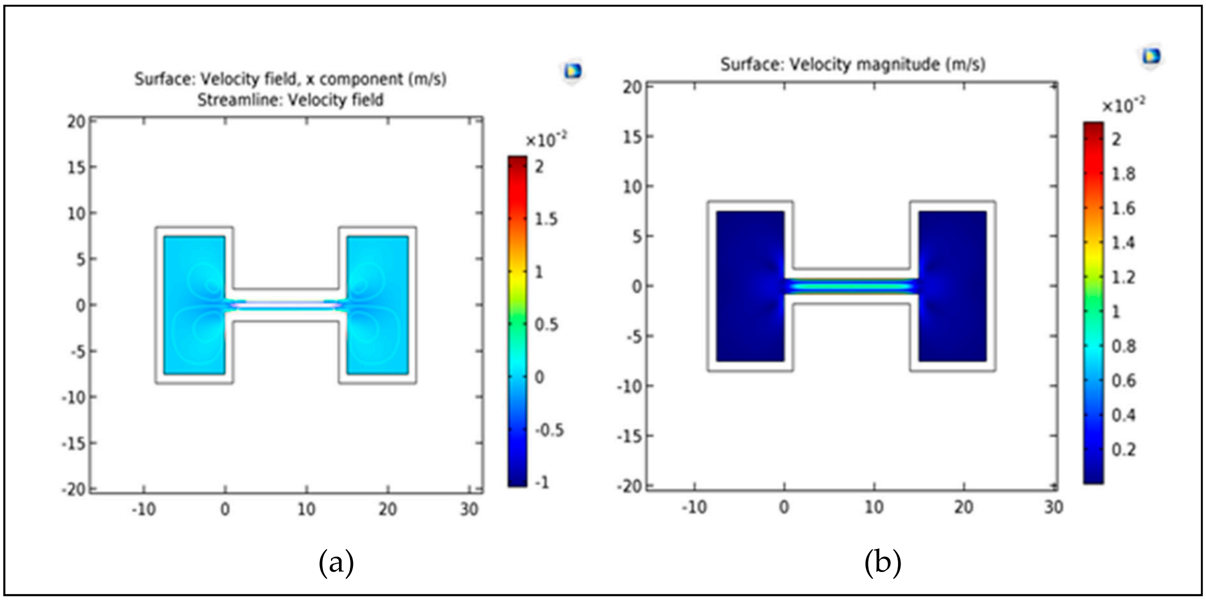

Figure 3: (a) Streamline velocity field v/s Channel length (b) Velocity Magnitude v/s Channel length

Figure 3 (a), shows a graph of streamline velocity field with respect to channel length. Figure 3 (b) shows a graph of velocity magnitude with respect to channel length. In the steady state there is no net flow through the channel, but a flow parallel to the walls, in the direction of the thermal gradient (cold to hot), develops due to thermal creep. In order to compensate for this flow, a back flow develops in the center of the channel, which is driven by a pressure gradient in the fluid. It results in a continuous flow of fluidic sample in the narrow micro fluidic channel. This is achieved by maintaining a constant pressure of 1 Pascal at the center of fluidic channel.

Figure 4 (a), shows fluid mean free path. Such rarefied flows are characterized by a parameter known as the Knudsen number, which is the ratio of the mean free path to the characteristic length of the geometry. Figure 4 (b), shows the relative pressure acting on the channel wall, as a function of position along the wall.

Figure 5 (a) and figure 5 (b) shows the temperature and pressure contours within the model. A temperature jump occurs between the vessel walls and the fluid normal heat fluxes occur into the wall from the fluid sample.

Preprints (www.preprints.org) | NOT PEER-REVIEWED | Posted: 23 November 2017 doi:10.20944/preprints201711.0154.v1

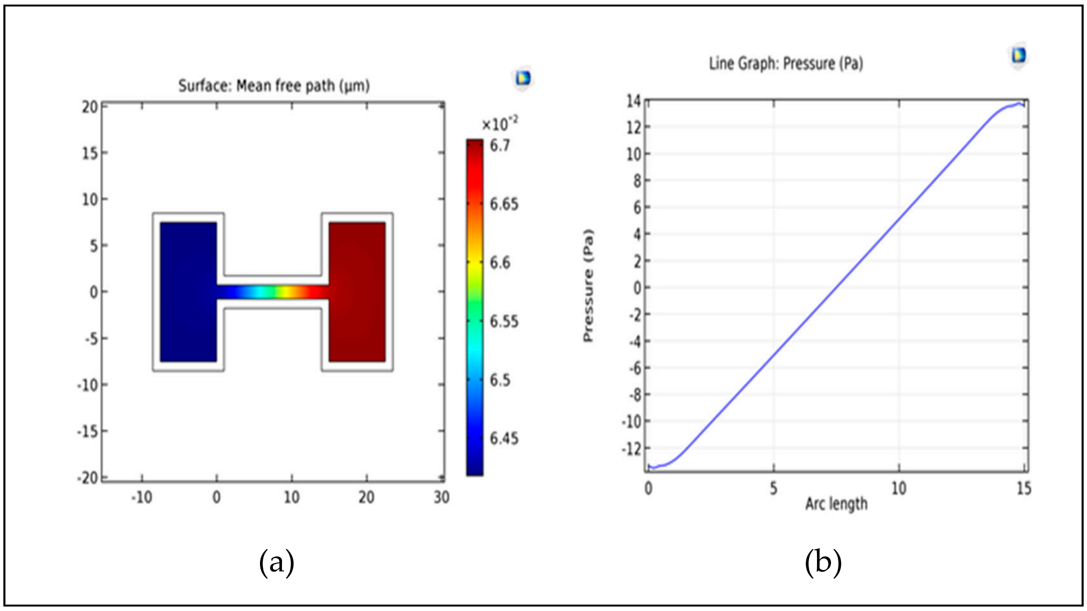

Figure 4: (a) Mean free path v/s Channel length (b) Pressure along channel length v/s Arc length

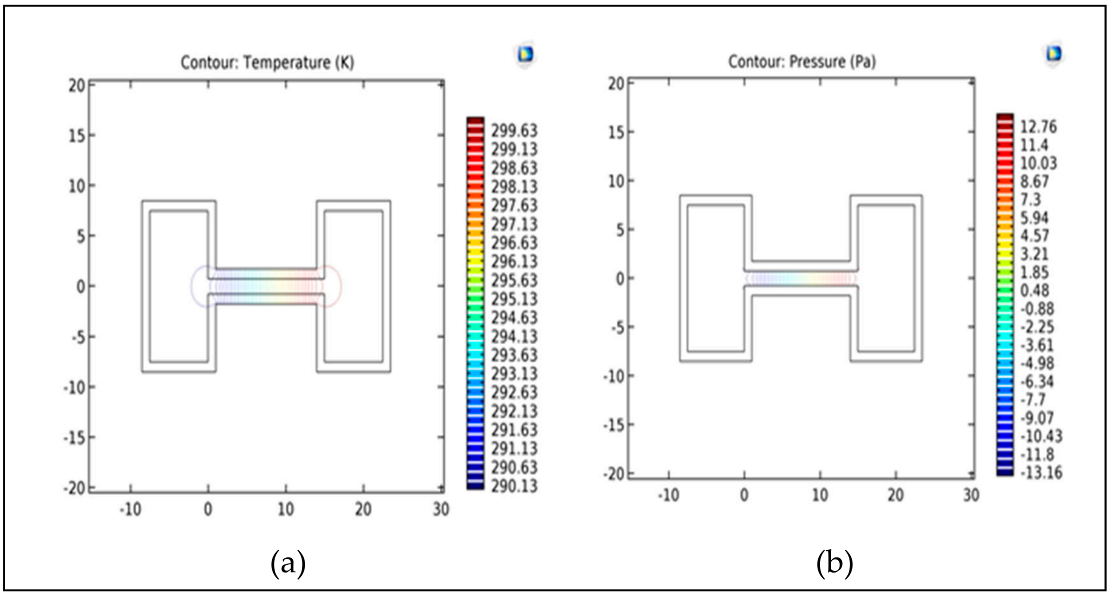

Figure 5: Contour diagram of (a) Temperature v/s Channel length (b) Pressure v/s Channel length

3. Modeling of SOI waveguide

In this section, the design and modal analysis of a single mode SOI waveguide structure to operate at a wavelength of 1550nm is presented. The SOI waveguide is designed at infrared region of light spectrum (1500nm-1600nm) for single mode operation.

Figure 6(a) shows the geometrical details of a SOI waveguide. It consists of silicon core having dimensions of 500nm width and 250nm height. These dimensions results in single mode operation. The substrate is silicon-di-oxide (SiO_2), which acts as lower cladding layer for the waveguide. The substrate height is designed for 2μm and width is designed for 4μm.

The dimensions and refractive index of the materials used in the waveguide geometry is shown in table1.

Preprints (www.preprints.org) | NOT PEER-REVIEWED | Posted: 23 November 2017 doi:10.20944/preprints201711.0154.v1

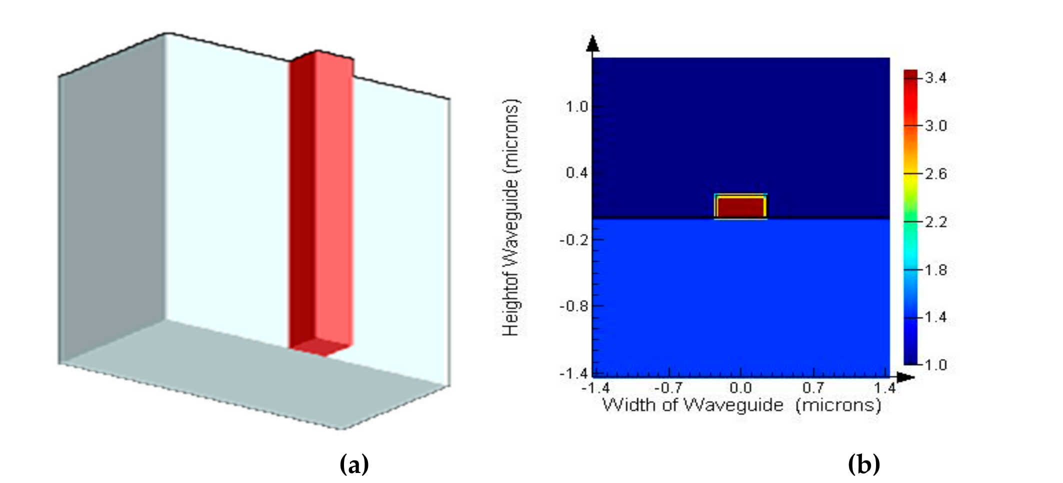

Figure 6: (a) Waveguide geometry (b) Refractive index distribution

Table 1: Materials and dimensions of waveguide

Material	Width (nm)	Height (nm)	Refractive Index at 1550nm
Si (Core)	500	250	3.4714
SiO2 (Substrate)	4000	2000	1.55

Figure 6 (b) shows the refractive index distribution of SOI waveguide (substrate (SiO_2), Core (Silicon) and Cover layer (Air)) at 1550nm.. There is a high refractive index contrast between silicon core (3.3714) and oxide substrate (1.55) index as well as cover layer (air) index. This high refractive index contrast results in SOI waveguides being highly amenable to light guiding at infrared wavelength. This results in excellent propagation characteristics such as dispersion, loss, effective index. The light confinement for various wavelengths in the range 1500nm to 1600nm is depicted in figure 7. It is observed that for all these wavelength range single mode operation is achieved with almost negligible loss.

Eigen mode (EM) solver is used for numerically simulate the waveguide geometry which is shown in figure. 6(a). The simulation settings used in the EM solver is shown in Table 2. Perfectly matched layers (PML) boundary conditions are used in the simulation [13].

Table 2: Eigen Mode Solver Settings

Parameter	Value
Mesh Resolution	50×50
Wavelength	1550nm-1600nm
Boundary conditions	PML
Background index	1 (Air)

Preprints (www.preprints.org) | NOT PEER-REVIEWED | Posted: 23 November 2017 doi:10.20944/preprints201711.0154.v1

4. Results and Discussion

In this section, the modal and power coupling analysis of opto fluidic sensor shown in figure 1 is presented. The sensor is designed to operate at 1550nm. It is observed that for 1500nm to 1600nm wavelength range single mode operation is achieved with excellent optical parameters and light confinement in input and output waveguides.

Figure 7 shows the optical mode confinement in SOI waveguide at 1550nm, 1530nm, 1550nm and 1600nm respectively. It is evident that the optical confinement of light is pronounced at the core of the waveguide (red color) when compared to the optical power leakage into the cladding (yellowish green color).Single mode operation is achieved for a core height of 250nm for the wavelength range 1500nm to 1600nm. In operation for bio-sensing application 1550nm is selected for the analysis. Figure 8 shows the magnetic field (H-field) intensity of SOI waveguide which is confined within the core region of waveguide. With the help of Figure 8, mode field diameter (MFD) is found out to be 1.774µm for a width of 0.5µm. Since MFD and width of the waveguide are of similar dimensions indicating very good optical mode confinement.

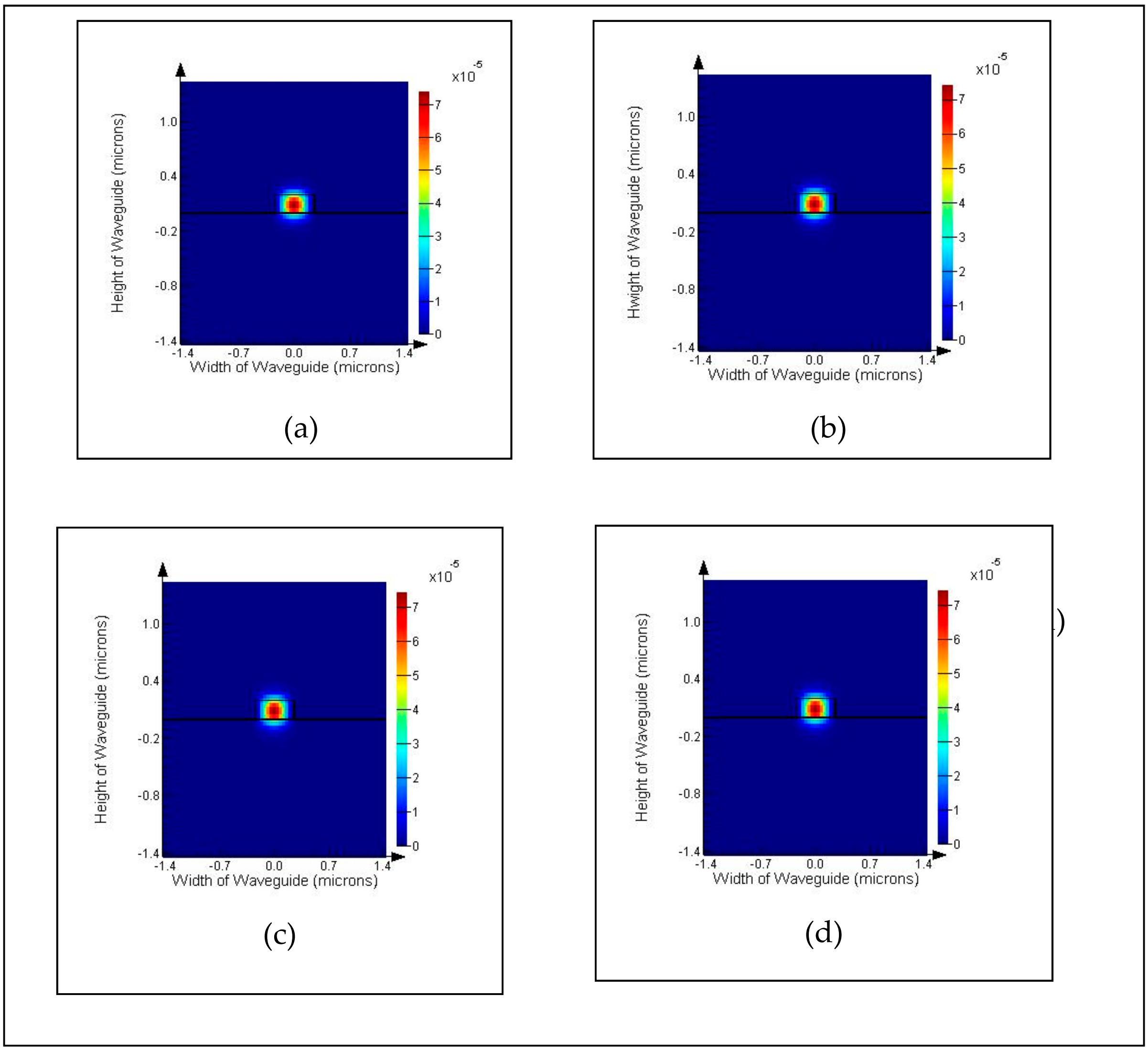

Figure 7: Mode Confinement Plots: TE0 mode confinement in a SOI waveguide at (a) 1500nm (b) 1530nm (c) 1550nm (d) 1560nm

Figure 9 and 10 shows the effective index and loss in SOI waveguide for a wavelength range of 1550nm to 1600nm. Table 3 gives the effective index, loss in dB/cm, percentage of TE/TM fraction for

Preprints (www.preprints.org) | NOT PEER-REVIEWED | Posted: 23 November 2017 doi:10.20944/preprints201711.0154.v1

the wavelengths 1550nm, 1530nm, 1550nm and 1600nm. Light and fluidic interaction is analyzed by considering fluidic region index as 1.334 (this approximately is refractive index of blood). The fluidic gap distance is designed is section 2 for 1.5µm. The input waveguide is excited by a laser source of 1550nm wavelength with 10dBm power level. The laser input power is coupled into the input waveguide the guided modes propagates through it and interacts with fluidic sample. Reflection of light takes place at the boundary between silicon core and fluidic sample. As a result the change in effective index occurs and the speed at which light propagates in the fluidic sample. This also results in variation of optical power intensity in the sensing region. Most of the light intensity is lost in the sensing region due to following optical phenomenons.

- Reflections of light into the substrate: It occurs due to low refractive index of fluidic sample (1.334) compared to substrate index (1.55).
- Absorption of light: It occurs due to the nature micro samples present in the fluidic sample. Absorption co-efficient and power intensity are related by Beers-Lambertz law [19].

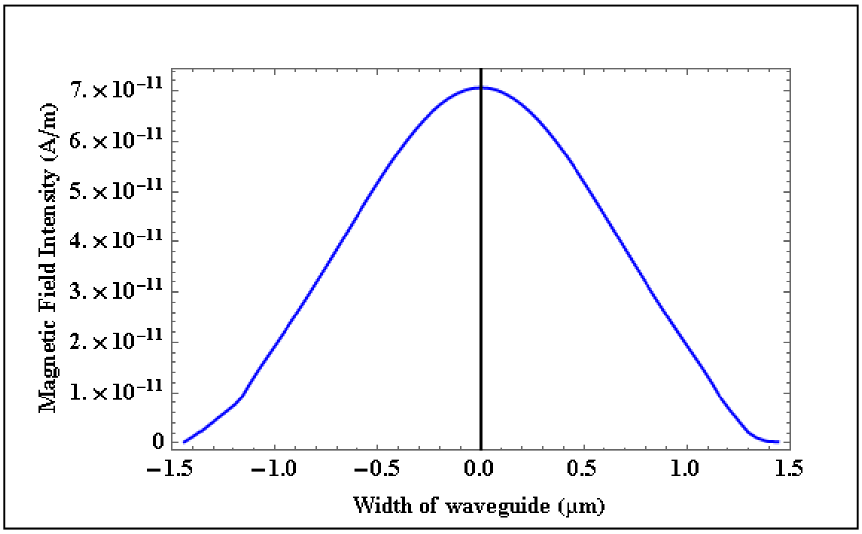

Figure 8: Magnetic field intensity as a function of width of waveguide

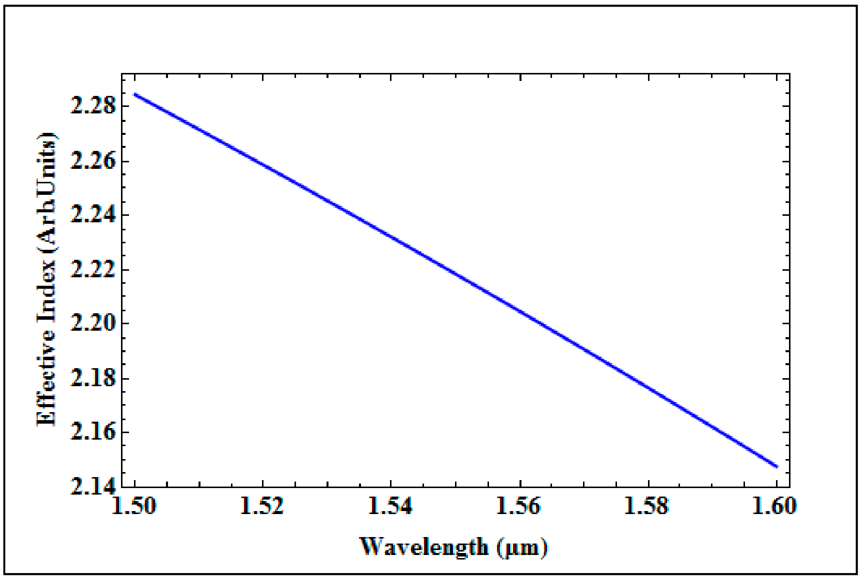

Figure 9: Effective Index as a function of wavelength

Preprints (www.preprints.org) | NOT PEER-REVIEWED | Posted: 23 November 2017 doi:10.20944/preprints201711.0154.v1

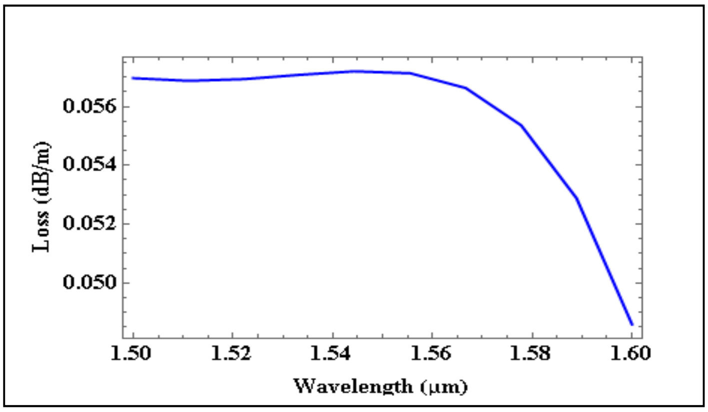

Figure 10: Loss in waveguide as a function of wavelength

Table 3: SOI Waveguide Parameter

Wavelength in nm	Effective Index	Loss in dB/cm	%(TE/TM) Fraction
1500	2.3619	0.000569	73.96/81.6
1530	2.322	0.00057	72.97/81.43
1550	2.2963	0.0005719	72.32/81.33
1600	2.230	0.00048597	70.75/81.1

The entire Lab-on-a-Chip structure as described in schematic representation of figure 1 and been simulated for optical mode propagation using 1550 nm source is shown in Figure 11. The optical power measurement analysis is carried out by considering input waveguide, output waveguide as mode waveguides with effective index 2.2963 and micro fluidic channel region as modal waveguide with effective index 1.383. The length of input and output waveguides is selected as 1mm and gap distance (fluidic channel width) is 1.5μm. The laser source wavelength is selected at 1550nm with a power level of 20dBm (1mW). The optical power of 19.999619 dBm is measured at the end of output waveguide using optical power meter. It indicates there is significant level of optical power coupling from input waveguide to output waveguide through the fluidic gap region. The optimum design parameters of the proposed sensor are listed in table 4.

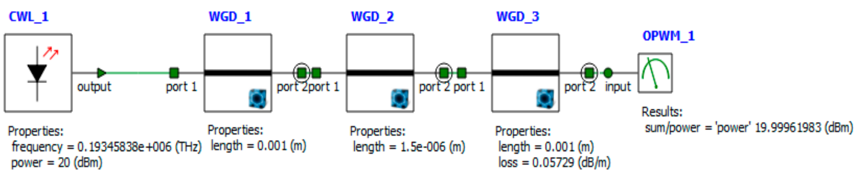

Figure 11: Optical power measurement using Interconnect

Table 4: Design parameters of opto-fluidic sensor

Parameter	Value
wavelength	1550nm
Height of input/output waveguide	250nm
Width of input /output waveguide	500nm
Width of fluidic channel	1.5μm
Length of input/output waveguide	1mm
Cross section of fluidic chambers	7.5 μm×15 μm

5. Conclusions

In this work modeling and analysis of integrated waveguides, and micro-fluidic channel for opto-fluidic lab-on-chip sensor application has been presented. The flow rate analysis between two fluidic chambers connected by a narrow micro fluidic channel which is in a plane perpendicular to integrated optical SOI waveguides is presented. The narrow fluidic channel sandwiched between two single SOI waveguides acts as a sensing region. A continuous flow of fluidic sample in the narrow micro fluidic channel is achieved by maintaining pressure of 1 Pascal at the centroid of the fluid channel geometry. The sensor is designed for single mode operation, which, is achieved at 1550 nm for waveguide dimensions of 250 nm (height) and 500 nm (width). The effective refractive index was found out to be 2.2963 with a negligible loss of 0.0005719dB/cm. It is observed that, when the input waveguide is excited by a laser source with 20dBm power at 1550nm, a power level of 19.999dBm is measured at the end of output waveguide. The power measured from output waveguide gives the qualitative measurement of optical properties and nature of the micro particles present in the fluidic sample. This micro structure fluidic channel with integrated laser and detector can be used for Bio-sensing applications.

Acknowledgments: The authors would like to thank Science and Engineering Research Board, Department of Science and Technology (DST-SERB) Grant Number YSS/2015/000382, Government of India for funding this research work.

Author Contributions: "Venkatesha M, Chaya B M and Narayan K conceived and designed the experiments; Venkatesha M performed the experiments; Venkatesha M, Narayan K, Chaya B M and Pattnaik P K analyzed the data; Narayan K contributed analysis tools; Venkatesha M and Narayan K wrote the paper."

Conflicts of Interest: The authors declare no conflicts of interest.

References

1. Volpatti L R, Yestisen A K, Commercialization of microfluidic devices, Trends in Biotechnology, 32(7), 347-350, 2014.
2. Saggiomo V, Velders H A,Sample 3D printed scaffold removal method for the fabrication of intricate microfluidic devices, Advanced Science, 2(8), 2015.
3. Ghallab Y, Badway W, Sensing methods for di-electrophoresis phenomenon from bulky instruments to lab on a chip, IEEE circuits and Systems Magazine, 4(3), 5-15, ISSN 1531-636X.
4. Ryan S Pawell, David W Inglis, Tracie J. Barber, and Robert A taylor, Manufacturing and wetting low cost microfluidic cell separation devices, Microfluidics, 7, 2013.
5. Tabeling P, Introduction to Microfluidics, Oxford University Press, 2015.
6. Chokkalingam V, Weidonhoff B, Kraener M, Maier W F, Herminghaus S, Seemann R, Optimized drop let-based microfluidics scheme for sol-gel reaction, Lab Chip, 10,2010.
7. Yuchan Zhang, Liang Su, Dan Manuzzi, Honorio Valdés Espinosa de los Monteros, Wenzhao Jia, Danqun Huo, Changjun Hou, Yu Lei, Ultrasensitive and selective non-enzymatic glucose detection using copper nanowires, In Biosensors and Bioelectronics, Volume 31, Issue 1, 2012, Pages 426-432, ISSN 0956-5663, https://doi.org/10.1016/j.bios.2011.11.006.
8. Alejandra Fernández-Cid, Alberto Riera, Pilar Herrero, Fernando Moreno, Glucose levels regulate the nucleo-mitochondrial distribution of Mig2, In Mitochondrion, Volume 12, Issue 3, 2012, Pages 370-380, ISSN 1567-7249, https://doi.org/10.1016/j.mito.2012.02.001.
9. Julaluk Noiphung, Temsiri Songjaroen, Wijitar Dungchai, Charles S. Henry, Orawon Chailapakul, Wanida Laiwattanapaisal, Electrochemical detection of glucose from whole blood using paper-based microfluidic devices, In Analytica Chimica Acta, Volume 788, 2013, Pages 39-45, ISSN 0003-2670, https://doi.org/10.1016/j.aca.2013.06.021.
10. Hyunggoo Park, Hyung Seo Yoon, Umakant Patil, Rani Anoop, Juho Lee, Juhwan Lim, Woonhyoung Lee, Seong Chan Jun, Radio frequency based label-free detection of glucose, In Biosensors and Bioelectronics, Volume 54, 2014, Pages 141-145, ISSN 0956-5663, https://doi.org/10.1016/j.bios.2013.10.053.
11. Yunhan Luo, Xiaolong Chen, Mengyun Xu, Zhe Chen, Xudong Fan, Optofluidic glucose detection by capillary-based ring resonators, In Optics & Laser Technology, Volume 56, 2014, Pages 12-14, ISSN 0030-3992, https://doi.org/10.1016/j.optlastec.2013.07.007.

Preprints (www.preprints.org) | NOT PEER-REVIEWED | Posted: 23 November 2017 doi:10.20944/preprints201711.0154.v1

12. Fernando Guerrero-Romero, Luis E. Simental-Mendía, Martha Rodríguez-Morán, Association of C-reactive protein Levels with Fasting and Postload Glucose Levels According to Glucose Tolerance Status, In Archives of Medical Research, Volume 45, Issue 1, 2014, Pages 70-75, ISSN 0188-4409, https://doi.org/10.1016/j.arcmed.2013.11.004.
13. A.L. Galant, R.C. Kaufman, J.D. Wilson, Glucose: Detection and analysis, In Food Chemistry, Volume 188, 2015, Pages 149-160, ISSN 0308-8146, https://doi.org/10.1016/j.foodchem.2015.04.071.
14. Chengcheng Liu, Yongjie Sheng, Yanhong Sun, Junkui Feng, Shijin Wang, Jin Zhang, Jiacui Xu, Dazhi Jiang, A glucose oxidase-coupled DNAzyme sensor for glucose detection in tears and saliva, In Biosensors and Bioelectronics, Volume 70, 2015, Pages 455-461, ISSN 0956-5663, https://doi.org/10.1016/j.bios.2015.03.070.
15. N.Y. Kim, R. Dhakal, K.K. Adhikari, E.S. Kim, C. Wang, A reusable robust radio frequency biosensor using microwave resonator by integrated passive device technology for quantitative detection of glucose level, In Biosensors and Bioelectronics, Volume 67, 2015, Pages 687-693, ISSN 0956-5663, https://doi.org/10.1016/j.bios.2014.10.021.
16. Guangran Ma, Min Yang, Chenyi Li, Haiyan Tan, Liang Deng, Shi Xie, Fugang Xu, Li Wang, Yonghai Song, Preparation of spinel nickel-cobalt oxide nanowrinkles/reduced graphene oxide hybrid for nonenzymatic glucose detection at physiological level, In Electrochimica Acta, Volume 220, 2016, Pages 545-553, ISSN 0013-4686, https://doi.org/10.1016/j.electacta.2016.10.163.
17. Wei Shen, Jun Sun, Jowy Yi Hoong Seah, Lei Shi, Sheng Tang, Hian Kee Lee, Needle-based sampling coupled with colorimetric reaction catalyzed by layered double hydroxide peroxidase mimic for rapid detection of the change of d-glucose levels with time in bananas, Analytica Chimica Acta, Available online 9 November 2017, ISSN 0003-2670, https://doi.org/10.1016/j.aca.2017.11.003.
18. Narayan. K, T. Srinivas, G. Mohan Rao and M. Manoj Varma, " Analysis of integrated optical lab-on-a-chip sensor based on refractive index and absorbance sensing", IEEE sensors J, 2013,13, (5) , pp. 1730-1741.
19. Berenger, J. A perfectly matched layer for the absorption of electromagnetic waves. J. Comput. Phys.1994, **114**, 185–200.
20. E.H. Kennard, Kinetic Theory of Fluides, McGraw-Hill, New York, 1938.
21. J.C. Maxwell, "On Stresses in Rarefied Fluides Arising from Inequalities of Temperature," Phil. Trans. R. Soc. Lond. **vol. 170**, pp. 231–256, 1879